Quantum interference in coherent tunneling through branched molecular junctions containing ferrocene centers

Xin Zhao,[1] Georg Kastlunger,[1,2] and Robert Stadler[1,*]

[1]*Institute for Theoretical Physics, TU Wien—Vienna University of Technology, Wiedner Hauptstrasse 8-10, A-1040 Vienna, Austria*

[2]*School of Engineering, Brown University, Providence, Rhode Island 02912, USA*

(Received 20 March 2017; revised manuscript received 9 June 2017; published 15 August 2017)

In our theoretical study where we combine a nonequilibrium Green's function approach with density functional theory we investigate branched compounds containing ferrocene moieties in both branches which, due to their metal centers, are designed to allow for asymmetry induced by local charging. In these compounds the ferrocene moieties are connected to pyridyl anchor groups either directly or via acetylenic spacers in a metaconnection, where we also compare our results with those obtained for the respective single-branched molecules with both meta- and paraconnections between the metal center and the anchors. We find a destructive quantum interference (DQI) feature in the transmission function slightly below the lowest unoccupied molecular orbital, which dominates the conductance even for the uncharged branched compound with spacer groups inserted. In an analysis based on mapping the structural characteristics of the range of molecules in our article onto tight-binding models, we identify the structural source of the DQI minimum as the through-space coupling between the pyridyl anchor groups. We also find that local charging in one of the branches changes the conductance only by about one order of magnitude, which we explain in terms of the spatial distributions of the relevant molecular orbitals for the branched compounds.

DOI: 10.1103/PhysRevB.96.085421

I. INTRODUCTION

Molecular electronics has become an active field of research in recent decades, since it holds the promise of maintaining continuous progress in the miniaturization of digital devices, thereby overcoming the limitations of semiconductor technology [1,2]. One enabling tool for this purpose can be found in destructive quantum interference (DQI) effects [3,4], which can significantly reduce the conductance in some conjugated π systems, where this purely electronic effect has also been shown to be robustly observable at room temperature [5]. For such hydrocarbon molecules a graphical atomic orbital (AO) scheme [6–10] as well as molecular orbital (MO)–based rules [11–16] could be derived to predict the occurrence of DQI from the molecular structure, where the relation between the two schemes has been clarified recently [17]. Such simplified schemes allow for the design of logical gates [6] and memory cells [18] in single-molecule electronics as well as the implementation of thermoelectric devices [19,20].

Also, the constructive quantum interference (CQI) expected in electron transport through branched molecular compounds has gained attention, where a deviation from the classical Kirchhoff's law was first predicted theoretically [21] and then confirmed experimentally [22,23] for junctions containing molecules providing symmetrically equivalent pathways through two of their branches. Recently, the design and synthesis of branched compounds containing ferrocene moieties in each branch have been presented [24] for the purpose of creating single-molecule junctions, where the combination of QI effects with redox gating for coherent electron tunneling as well as the electrostatic correlation between spatially distinct redox centers for electron hopping [25] can be explored.

The latter electrostatic interactions between multiple ferrocene-based redox centers within the same compound have been observed in an unrelated study [26]. Ferrocene moieties in junctions with linear molecules [27] have also been used for the design of molecular diodes [28–30], highly conducting molecular wires [31], and redox-gated molecular switches [32], where the switching between a low-conductance reduced state and a high-conductance oxidized state was due to stochastic fluctuations between these two redox states induced by the gate. The details of the mechanism for this type of switching have recently been explored in joint experimental and theoretical studies on a Mo compound [33,34] and azulene [35], where the *I/V* curves measured in a mechanically controlled break junction setup were also reproduced by simulations based on density functional theory (DFT).

The novelty of the molecular design in Ref. [24] lies in bringing all these structural aspects together in a single molecule, which could, in principle, allow to combine redox-gated fluctuations of the electron population at ferrocene moieties as a switching mechanism between two redox states, where DQI effects would guarantee a very low conductance for one of them, and their absence a significantly higher conductance for the other one. A similar idea for a redox-gated switch, where one state of the redox pair was designed to exhibit DQI effects, has recently been pursued with anthraquinone derivatives but the on/off ratios were found to be rather modest, since DQI occurred rather far in energy from the Fermi level (E_F) in the transmission function [36]. Although the synthesis part in Ref. [24] focused on branched compounds where both branches were to be attached on a substrate separately and only connected intramolecularly by a pyridyl anchor group on the end to be contacted by the tip of a scanning tunneling microscope, the authors stated in their conclusions that efforts towards cyclic analogs of these molecules such as the one shown in Fig. 1 were under way.

*robert.stadler@tuwien.ac.at

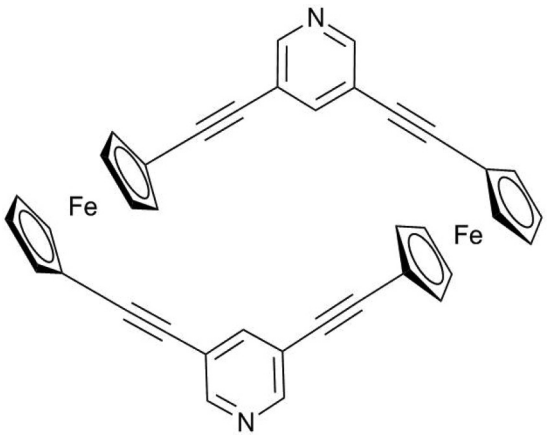

FIG. 1. Cyclic molecule containing a ferrocene moiety in each of its two branches, where they have been separated from the pyridyl anchor groups by acetylenic spacer groups.

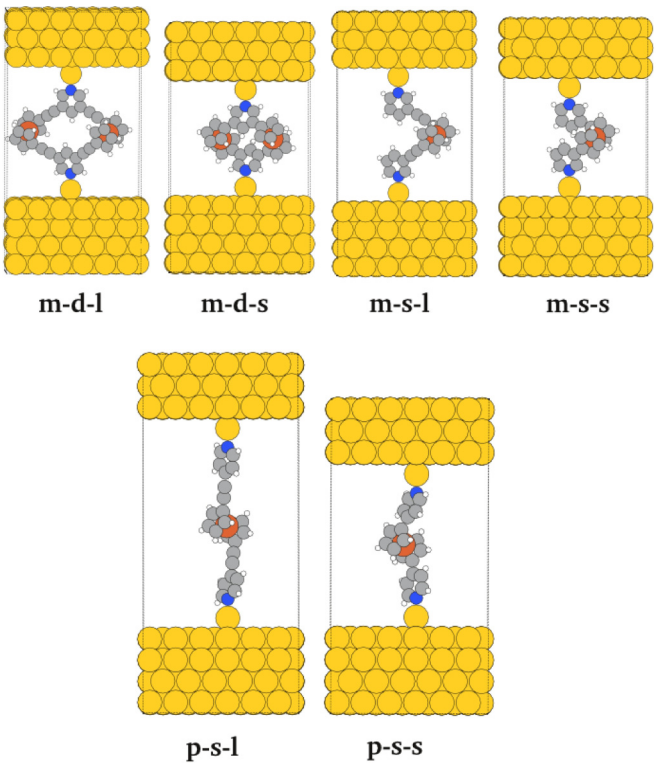

FIG. 2. Junction geometries for the compounds we investigate in this article. m-d-l (meta-double-long) denotes the molecule in Fig. 1; m-d-s (meta-double-short), the same molecule without the acetylenic spacer groups; m-s-l (meta-single-long) and m-s-s (meta-single-short), the corresponding single-branched compounds; and p-s-l (para-single-long) and p-s-s (para-single-short), their respective counterparts with a para-connection to the pyridyl anchor groups. All molecules have been connected to fcc Au electrodes on (111) surfaces with an adatom on each lead.

Such cyclic analogs are of particular interest in the context described above, since as pointed out in Ref. [22], QI effects can only be expected to play a dominant role for electron transport if both sides of a branched molecule are connected to electrodes by a common intramolecular node. For the molecule in Fig. 1 in its neutral state the transmission through both branches is expected to interfere constructively, because the branches are symmetry equivalent [21–23]. If one of the two ferrocene moieties is oxidized, however, this symmetry will be brokenm thereby possibly enabling a DQI-induced suppression of the conductance. In that case the compound in Fig. 1 could be used as a molecular redox switch with very high on/off ratios. In the molecular design the acetylenic spacers are meant to make the molecular structure more rigid and to increase the distance between the two electrodes for the prevention of through-vacuum tunneling and for the separation of the redox-active centers from the leads. The pyridyl anchor groups were chosen because they were found to provide the best junction formation and conductance properties in recent experimental [37] and theoretical [38–41] studies.

In our article we investigate the coherent electron transport through the molecule in Fig. 1 by means of DFT calculations in combination with a nonequilibrium Green's function (NEGF) formalism [42], where we put an emphasis on DQI effects in neutral and charged compounds. Because of the presence of the ferrocene moieties in the compound neither the graphical AO scheme nor the MO rules mentioned above can be applied for this purpose, since both have been designed exclusively for the study of π conjugated hydrocarbons [17], which is also true for the quantum circuit rules derived in Ref. [43]. In the present case, however, DQI can arise (i) from the metaconnection [44–46] of the branches to the pyridyl anchor group, although it has recently been demonstrated that for meta-connected bipyridine DQI in the π-electron contribution can be masked by the conductance mediated by σ electrons [47]; (ii) from interference between transmission through the two branches, which is expected to be constructive for the neutral molecule but might be destructive if the redox-active center on only one of the branches is oxidized; and (iii) from multiple paths provided by nearly degenerate orbitals on the ferrocene moieties. In order to be able to distinguish these effects we extend our study to the range of molecular junctions illustrated in Fig. 2, where, derived from the compound in Fig. 1, we also chose molecules without acetylenic spacers, with only one branch between the pyridyl anchor groups and with paraconnections for the single-branched systems.

The paper is organized as follows: In the next section we present transmission functions from NEGF-DFT [48–51] calculations for all junctions in Fig. 2 and discuss their characteristic features. There we find that DQI occurs for neutral compounds in the energy region of the lowest unoccupied MO (LUMO) close to the Fermi level, with a strong impact on the conductance only for molecules with branches connected in metapositions at the pyridyl anchors with respect to their N atom and containing acetylenic spacers regardless of the number of branches, i.e., for the compounds we refer to as m-d-l and m-s-l in the caption to Fig. 2. In Sec. III we derive topological tight-binding (TB) models from the DFT calculations and identify the through-space coupling between the pyridyl anchor groups, which depends on both the meta- versus paraconnectivity and the presence or absence of spacer groups as the defining quantity for the DQI effects we observe. In Sec. IV we assess the usefulness of the double-branched systems m-d-l and m-d-s in Fig. 2 as molecular switches

by explicitly putting a positive charge on one of the two branches in our NEGF-DFT calculations and comparing the resulting conductance with that of the respective neutral compound. We conclude with a brief summary of our results in Sec. V.

II. DFT-BASED ELECTRON TRANSPORT CALCULATIONS AND MOLECULAR ORBITALS FOR NEUTRAL COMPLEXES

A. Computational details for NEGF-DFT calculations

We obtained the transmission functions $T(E)$ for all junctions in Fig. 2 from NEGF-DFT calculations performed with the GPAW code [52,53] using a linear combination of atomic orbitals (LCAO) [54] for the basis set on a double-zeta level with polarization functions (DZP), a Perdew-Burke-Ernzerhof (PBE) parametrization for the exchange correlation (XC) functional [55], and a grid spacing of 0.2 Å for the sampling of the potential in the Hamiltonian on a real-space grid. In our transport calculations, the "extended molecule" defining the scattering region is formed by the respective metal organic compounds and three and four layers for the upper and lower fcc gold electrodes, respectively, in a (111) orientation and with a 6×6 overstructure defining the periodically repeated unit cell, where the distance between the Au adatom attached to the lead surfaces and the N atom of the pyridyl anchor groups was chosen as 2.12 Å [38] and a k-point sampling corresponding to a $4 \times 4 \times 1$ Monkhorst Pack grid for evaluating $T(E)$, where the z coordinate is the direction of electron transport through the junction.

B. Transmission functions from NEGF-DFT and the observation of DQI

In the resulting transmission functions in Fig. 3 the peaks in the LUMO region are much broader than those in the HOMO region for all systems, and hence we expect the conductance to be dominated by the MOs above the Fermi level. DQI-induced minima in the energy region at the upper border of the HOMO-LUMO gap can be observed only for metaconnected molecules with acetylenic spacers regardless of the number of branches but this feature disappears when the spacers are removed or when the connection of the ferrocene moieties to the pyridyl anchors is in a para position. We note that these minima in $T(E)$ in the LUMO region for the compounds m-d-l and m-s-l do not result in zero conductance accompanied by the typical DQI shape known from topological models [17] but rather in a distinct deviation from Lorentzian decay around the LUMO peaks, which lowers the conductance significantly and has been encountered in molecules with metaconnected pyridyl anchors also in Ref. [43].

These less distinctly visible manifestations of DQI can occur in DFT calculations for real systems, because DQI is linked to the symmetry properties of π electrons of a conjugated system, where σ electrons are not necessarily affected [47]. Our definition of DQI is that the transmission through a system with more than one MO around E_F is lower

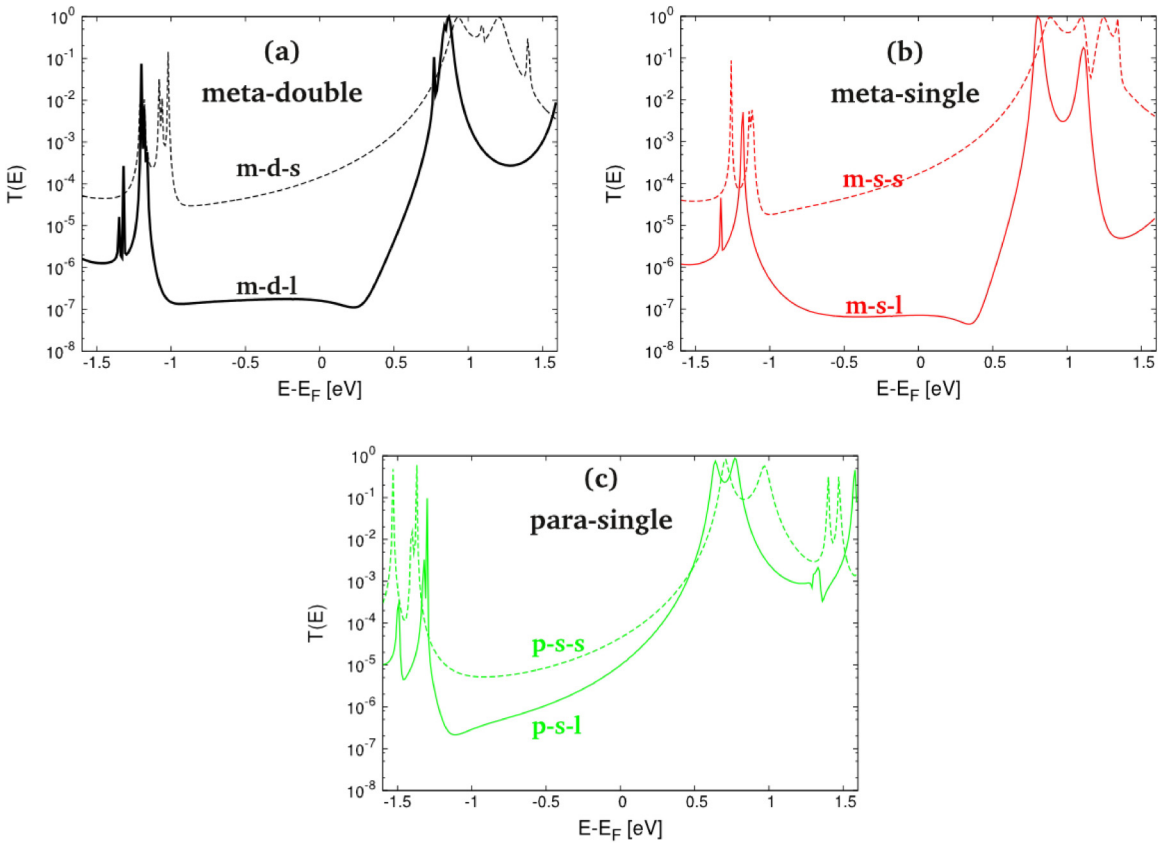

FIG. 3. Transmission functions calculated from the NEGF-DFT for the six junctions in Fig. 1. (a) m-d-l, solid black line; m-d-s, dashed black line. (b) m-s-l, solid red line; m-s-s, dashed red line. (c) p-s-l, solid green line; p-s-s, dashed green line.

than the sum of the individual contributions of these MOs to $T(E)$ [40]. The exact energetic position of the Fermi energy within the HOMO-LUMO gap, which is also affected by the underestimation of this gap in our calculations due to the PBE parametrization of the XC functional, will have a crucial impact on the quantitative conductance, but qualitatively DQI will always result in a significant conductance lowering for the structures where it occurs regardless of the details of the Fermi level alignment [17].

C. General remark on CQI for the branched molecules

From the circuit laws derived for branched molecules with two equivalent branches [21,22], one would expect that due to constructive QI the conductance of the molecules would be roughly four times as large as the respective value for the single-branched analog. While for molecules containing acetylenic spacers we indeed find a ratio greater than 2 between the respective transmission functions of m-d-l and m-s-l at E_F in Fig. 3, this is distinctly not the case for m-d-s and m-s-s, where the conductance of the single-branched system is even slightly higher than that found for the double-branched compound. In Refs. [4,21] it was pointed out that the circuit laws for CQI only apply when the branches are rather weakly coupled to the nodal point in comparison with the nodal point's electronic connection to the electrodes. In our case, however, the coupling between the ferrocene moieties and the pyridyl anchors is larger than the coupling between the anchors and the leads. In the experimental evaluation of the circuit laws for CQI in Ref. [23] it was also found that the observability of these laws strongly depends on the chemical nature of both the anchors and the branches as well as on the atomistic details of the surface structure the respective compounds are attached to.

D. Molecular orbital analysis

In Figs. 4 and 5 we plot the spatial distributions of the MOs for the double-branched compounds directly above (Fig. 4) and directly below (Fig. 5) the Fermi energy, which we obtain from a subdiagonalization of the molecular part of the transport Hamiltonian [41]. In Table I the corresponding eigenenergies are listed for all six junctions in Fig. 2, where the lists are complete for the energy range $-2\ \text{eV} < E_F < 1.5\ \text{eV}$ and the shapes of MOs for the single-branched systems share

TABLE I. Eigenenergies ϵ_{MO} (in eV) for the four MOs above E_F (LUMO,...,LUMO + 3) for all compounds in Fig. 3 and the three MOs below E_F (HOMO,...,HOMO − 2) for one of the two branches. For m-d-l and m-d-s the values for the respective second branch are given in parentheses.

	m-d-l	m-d-s	m-s-l	m-s-s	p-s-l	p-s-s
L + 3	0.85	1.39	1.08	1.33	1.32	1.46
L + 2	0.81	1.17	1.06	1.21	1.28	1.39
L + 1	0.79	1.09	0.78	1.07	0.70	0.91
L	0.76	0.86	0.76	0.81	0.57	0.64
H	−1.16 (−1.20)	−1.02 (−1.06)	−1.18	−1.12	−1.30	−1.37
H − 1	−1.18 (−1.21)	−1.02 (−1.08)	−1.19	−1.14	−1.32	−1.41
H − 2	−1.32 (−1.35)	−1.18 (−1.21)	−1.33	−1.26	−1.49	−1.53

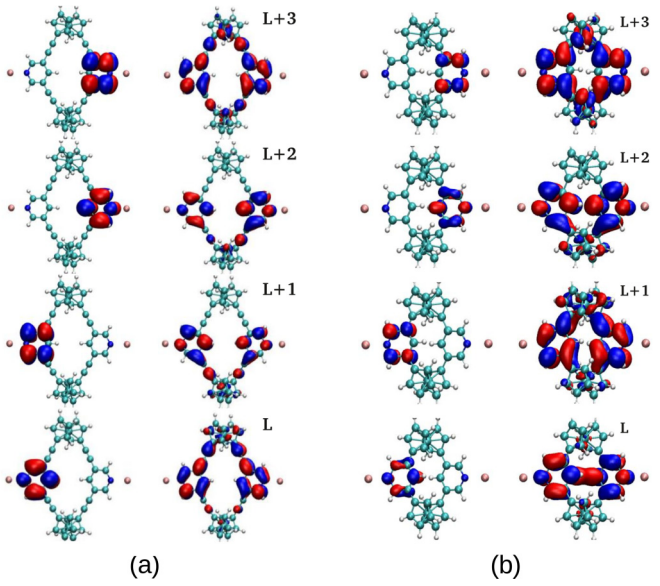

FIG. 4. Spatial distributions of the four MOs directly above E_F (LUMO,...,LUMO + 3) for the branched compounds (a) m-d-l and (b) m-d-s; the two FOs on each pyridyl anchor defining them are shown in the left columns, and the four MOs themselves in the right columns.

the same localization patterns with those plotted for the double-branched molecules in Figs. 4 and 5. For the LUMO region all four MOs are mostly localized on the pyridyl anchor groups (Fig. 4), which explains the broad peaks found for all junctions in $T(E)$ above E_F (Fig. 3). Furthermore, visual inspection allows us to identify these four MOs as bonding or antibonding pairs resulting from the hybridization of just two pyridyl fragment orbitals (FOs), which were again obtained from a subdiagonalization of the respective transport Hamiltonian, but in this case limited to the basis functions centered on the pyridyl groups.

The MOs below E_F on the other side (Fig. 5) are all mostly localized on the ferrocene moieties as hybrids of Fe d states

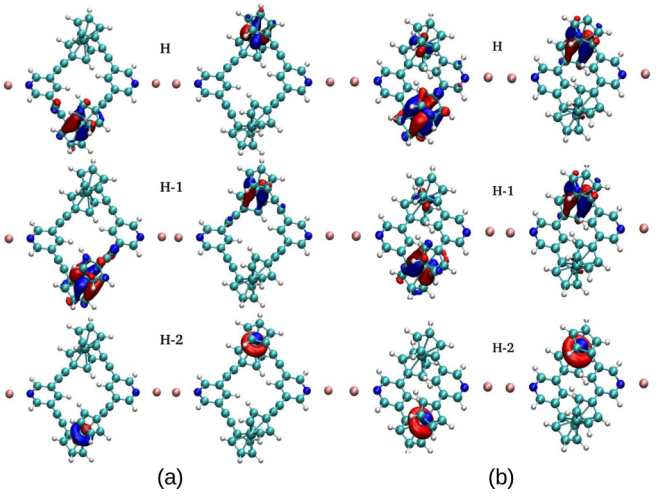

FIG. 5. Spatial distributions of the six MOs directly below E_F (HOMO,...,HOMO − 5) for the branched compounds (a) m-d-l and (b) m-d-s; the notation we use here (H,...,H − 2) refers to each branch individually.

and the π system of their cyclopentadienyl rings. As a result we observe rather narrow peaks of $T(E)$ in the HOMO region (Fig. 3) at all junctions. For the double-branched compounds, these six MOs can be clearly separated into three on each branch, suggesting that our initial concept of introducing a positive charge at one ferrocene center for the creation of an asymmetry resulting in DQI might work for $T(E)$ in the HOMO region. It is, however, not likely to be applicable in the LUMO region since the localization patterns in the pyridyl anchors cannot be expected to be affected in an asymmetric way by the charging of one ferrocene moiety. In order to evaluate the validity of this first assessment further, NEGF-DFT calculations with explicitly charged ferrocene centers are presented in Sec. IV.

Since both the shapes and the eigenenergies (as listed in Table I) of all MOs are quite similar for the six junctions in Fig. 2, it cannot be directly derived from these properties why a DQI feature occurs in $T(E)$ in the LUMO region for compounds m-s-l and d-s-l but not for the other four molecules in Fig. 3. It might be expected that the number of branches does not make a difference here because the existence of the second branch should induce CQI but not DQI without the charging of a ferrocene center [21–23]. It also seems intuitive that molecules, where ferrocene is connected to the pyridyl anchors in metaconnections exhibit DQI, while the para-analog does not but this intuition is only based on the observations made for planar π-conjugated hydrocarbons [44,45], while the six compounds in Fig. 2 are not planar and contain ferrocene moieties. Most strikingly, there is no easy explanation for the dependence of the DQI feature on the absence or presence of acetylenic spacers. In order to investigate these questions further, we project the data we can derive from NEGF-DFT calculations onto topological TB models in Sec. III.

III. INVESTIGATION OF THE STRUCTURAL SOURCES OF DQI WITH TB MODELS

All conventional topological TB models and the various sets of QI or quantum circuit rules derived from such models have been developed for planar π-conjugated hydrocarbons. Also, the simple assertion that metaconnected junctions exhibit DQI, while paraconnected ones do not, can be considered to be a simple case of a QI rule derived from a conventional topological TB model. In such models the molecular structure is replaced by a connectivity matrix where each carbon position is represented by a single AO (presumably the p_z orbital perpendicular to the plane), where all AOs have the same on-site energy and only next-neighbor couplings are considered. The ferrocene makes both assumptions ambiguous. It cannot be represented by carbon p_z AOs alone but has degenerate FOs at different energies instead. Additionally, it enforces molecular structures in three dimensions in deviation from planarity, where parts of the molecule not directly bonded to each other can come close to each other in the third dimension and QI can no longer be understood in terms of next-neighbor connectivity alone. As conventional TB models are not applicable for the structures we investigate, we have to derive our own models, which must fulfill two requirements: (i) the qualitative structure dependence of the transmission functions from our DFT calculations needs to be reproduced, and (ii) the number of orbitals involved at the end needs to be minimal in order to make the key structural source of DQI in our systems discernible. This step-by-step model development is introduced in this section and the applicability of the procedure is not limited to the particular six molecules we investigate but is also given for similar systems.

For double-branched molecules the transmission functions in Fig. 3 have a shape very similar to that of their respective single-branched analogs in the LUMO region in metaconnected cases, and the acetylenic spacers do not seem to have a significant impact on paraconnected anchors other than the well-known decrease in conductance with molecular length. Therefore, we focus our analysis of the relationship between structural features and $T(E)$ in this section on an evaluation of the differences between compounds m-s-l, m-s-s, and p-s-l.

A. Definition of the electrodes for all NEGF-TB calculations

We calculate transmission functions from NEGF-TB with a one-dimensional chain of AOs acting as electrodes, where all inner-electrode on-site energies have been set to 0.83 eV and all inner-electrode couplings to −5.67 eV. This particular choice for the latter two parameters has been identified as optimal for reproducing NEGF-DFT results for $T(E)$ with fcc Au (111) electrodes in Ref. [40] and is used for all NEGF-TB calculations in the current article. The couplings between the contact atoms of these artificial electrodes and the p_z orbitals within the pyridyl anchors have been derived by a subdiagonalization of the part of the transport Hamiltonian from the NEGF-DFT calculations describing the gold adatoms on top of the surfaces (see Fig. 2) and taking only the couplings of the valence s state of this atom to the pyridyl p_z states because the density of states of the gold surface has a predominantly s character around E_F.

B. Selection of AOs in the anchor groups and FOs in the ferrocene for reproducing the DFT results

In the first part of this analysis we try to map the structural characteristics of these three molecules onto a topological TB model, with the aim of matching the $T(E)$ from NEGF-DFT as closely as possible but at the same time minimize the number of involved orbitals. For the pyridyl anchors and acetylenic spacers it can be safely assumed that transport near the HOMO-LUMO gap is dominated by the p_z AOs at the C and N sites [40]. The DZP-LCAO basis set of the NEGF-DFT calculations, however, does not provide physically meaningful AOs, in particular, atoms in the environment of all neighboring atoms. Hence, we obtained the basis which we need to apply in our TB models by subsequent subdiagonalizations and basis set rotations of the transport Hamiltonian for each C and N atom individually. [47] Additionally, orthogonality between AOs on neighboring atoms was ensured by applying a Löwdin transformation [56]. As it has been demonstrated in the supporting information in Ref. [47] that not only first- but also second- and third-nearest-neighbor couplings within a pyridyl group are crucial for defining the energetic position of a DQI minimum, we include all three categories in our model. For the ferrocene part of the molecules we perform a subdiagonalization of the part of the Hamiltonian covering the

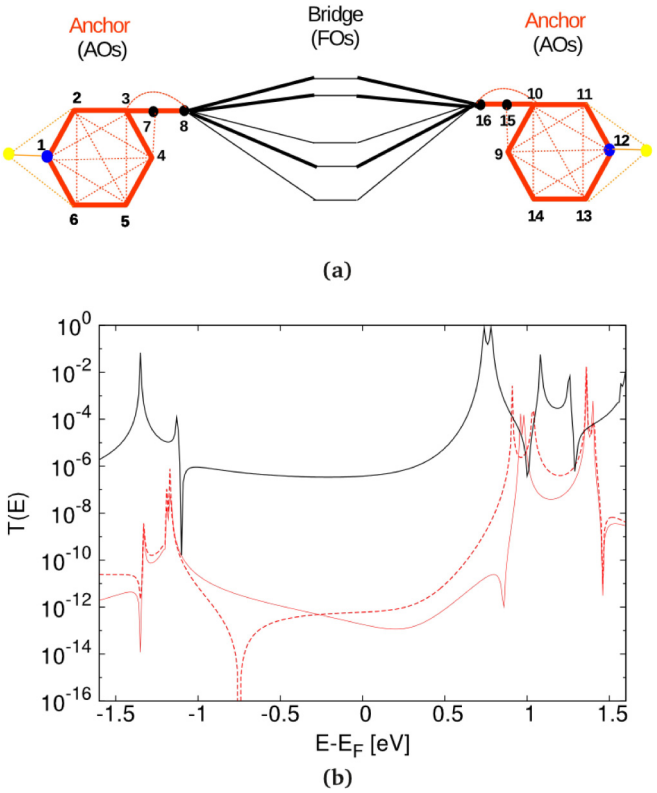

FIG. 6. (a) TB model derived from the NEGF-DFT as exemplified for compound m-s-l, where the line colors distinguish between couplings within anchors and spacers (red) and couplings to ferrocene FOs (black) or the gold leads (yellow), respectively, while the line thickness illustrates the hierarchy of the respective coupling strengths. (b) $T(E)$ from the TB model for m-s-l, with (dashed red curve) and without (solid red curve) an artificially high value for the direct coupling, and for m-s-s (solid black curve).

whole moiety, which results in just five FOs in the relevant energy range around the HOMO-LUMO gap, namely, three FOs with energies from −1.55 to −1.20 eV in the HOMO region and two FOs with energies from 1.35 to 1.55 eV in the LUMO region for all three compounds.

In Fig. 6(a) we illustrate this TB model schematically for molecule m-s-l; direct couplings between the p_z orbitals of anchor and spacer groups left and right of the ferrocene are not drawn for the sake of simplicity but still considered in the model.

C. Identification of the through-space coupling between anchor groups as the structural source of DQI

Since we know that the most distinct structural difference between the m-s-l and the m-s-s molecules lies in their respective molecular lengths, as brought about by the presence or absence of acetylenic spacers, we show in Fig. 6(b) the $T(E)$ from NEGF-TB for m-s-l in the original parametrization as derived from DFT (solid red line) and with just one parameter changed to the higher value we obtain for m-s-s (dashed red line), namely, the direct coupling between AO 4 and AO 9 in Fig. 6(a). Of course, this "artificial" parametrization, which is meant to mimic a key structural aspect of m-s-s does not reproduce the high conductance found for this system in Fig. 3 but it can be clearly seen that just changing this one parameter from the value it has in m-s-l to the one it has in m-s-s seems to be sufficient to shift the DQI feature so far down in energy that it is no longer observable in the LUMO region. In Fig. 6(b) we also plot the transmission function we obtain from the parameters and topology of compound m-s-s (solid black line), which, just like the one for m-s-l (solid red line), perfectly reproduces all characteristics found from NEGF-DFT in Fig. 3. The model, however, needs to be simplified further in order to pin down and separate the effects of the most important structural differences between the single-branched molecules.

For that purpose we perform another subdiagonalization of the transport Hamiltonian in the subspace of the eight p_z AOs on the pyridyl anchors and acetylenic spacers in Fig. 6(a) on each side of the ferrocene center. This results in the FO-TB model in Fig. 7(a), where the five FOs on the ferrocene moiety are the same as in Fig. 6(a) and two FOs on each anchor can be roughly identified from their shape with those shown in Fig. 4(a), albeit they now show some localization on the spacer groups too due to the manner of their definition. From the size of the couplings of the five bridge FOs to these two anchor FOs we can identify the three bridge FOs most relevant for the m-s-l molecule, namely, one in the HOMO region and two in the LUMO region as indicated in Fig. 7(a), while for p-s-l only the bridge FO lowest in energy in the LUMO region and only the lower lying of the two FOs on the anchors plays a role for the transmission.

Molecules m-s-l and p-s-l now differ in the FO-TB model in two ways, namely, in the number of FOs on each of the three fragments connected by sizable couplings and in the detailed values for these couplings. Therefore, the question arises whether DQI in $T(E)$ would still be found for compound m-s-l if only the one FO on each fragment also relevant for the p-s-l system but with the parameters for m-s-l (Fig. 7b) is selected for NEGF-TB calculations with a minimal number of FOs. In Figs. 7(c) and 7(d), we present the results of such calculations. Figure 7(c) shows the $T(E)$ for molecule m-s-l with two anchor FOs on each side and five (solid line), three (dashed line), and one (dotted line) FO on the ferrocene, respectively, and it can be seen that the DQI feature is shifted to the HOMO region if the quality of the FO model is reduced but remains observable. In Fig. 7(d) we choose the same single FO on each fragment setup for compounds m-s-l (red curve) and p-s-l (green curve) as illustrated in Fig. 7(b), where we come to the somewhat surprising conclusion that DQI is still observed for m-s-l but not for p-s-l, although the models for the two systems now differ only in the detailed parameters for the couplings between three FOs which have very similar spatial distributions and on-site energies in both cases.

D. Analysis of the mathematical reasons for the decisive influence of the through-space coupling with a simplified 3 × 3 Hamiltonian

In Table II we list the coupling values for t_L, t_R, and t_D connecting the three FOs in Fig. 7(b) for all three junctions, where the first two parameters do not vary with the molecular structure significantly but the third one does. Having now established that the direct coupling between the two anchor

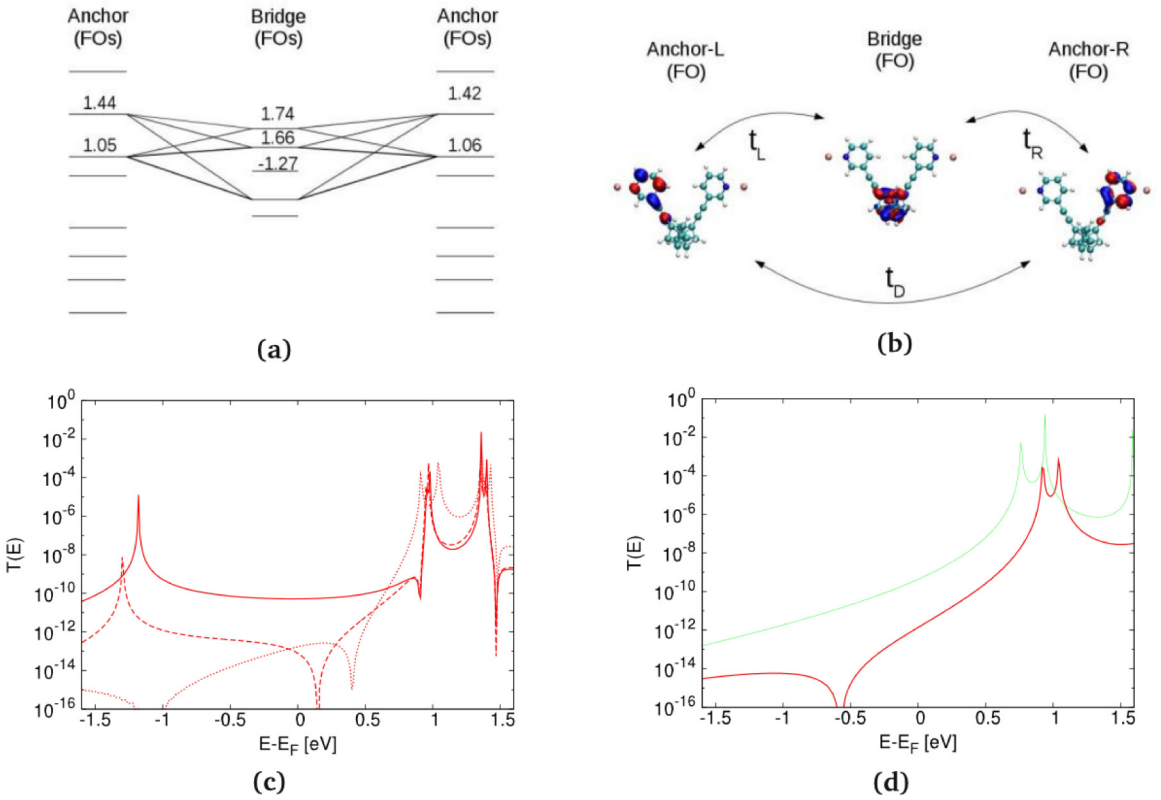

FIG. 7. (a) FO-TB model for molecule m-s-l as described in the text, where the relevant couplings between anchor and bridge states which are all in the range of 0.1–0.2 eV are indicated by lines. (b) Spatial distributions of the anchor FO on each side at 1.05 eV and the ferrocene FO at 1.66 eV. (c) $T(E)$ as calculated from the NEGF-TB for this model are shown as red lines for two anchor FOs [as marked in (a)] and all five bridge FOs (solid red line), only three bridge FOs [as marked in (a); dashed red line], and only the one bridge FO at 1.66 eV (dotted). (d) $T(E)$ or compound m-s-l (red line) and p-s-l (green line) for only the one anchor FO on each side and one bridge FO in the middle as plotted in (b).

groups distinguishes the only single-branched system with a DQI feature close to the LUMO, namely, molecule m-s-l, from both compound m-s-s and compound p-s-l, we want to explore the mathematical reasons for the importance of this parameter. We therefore diagonalized a 3×3 Hamiltonian with fixed parameters for the three FOs in Fig. 7(b) and plotted the evolution of the resulting three MOs in dependence on t_D in Fig. 8(a). In Fig. 8(b) we show the transmission functions for selected values of t_D, which we obtained by making use of Larsson's formula [57],

$$\Gamma(E) = \sum_i \frac{\alpha_i \cdot \beta_i}{E - \varepsilon_i}, \tag{1}$$

where ε_i is the eigenenergy of each MO, and α_i and β_i are its respective couplings to the left and right electrodes.

TABLE II. Couplings connecting the three FOs in Fig. 7(b) for three of the single-branched systems; all values are eV.

	Coupling		
	m-s-l	p-s-l	m-s-s
t_L	0.27	− 0.23	− 0.28
t_R	− 0.22	0.25	0.22
t_D	− 0.023	− 0.0087	0.033

Larsson's formula was originally introduced for the definition of the transfer integral in the context of Marcus theory for the description of electron hopping [57–59], but recently it has been shown that it can also be used to approximate $T(E)$ as $T(E) \sim \Gamma^2(E)$ for coherent tunneling [40,60], where the resulting $T(E)$ can be normalized [60] and qualitatively reproduces the curves obtained from NEGF-TB [17].

Equation (1) has the additional advantage that a simple mathematical condition can be defined for the energetic positions of DQI-induced zeros in $T(E)$, because at the same energies the effective coupling $\Gamma(E) = \gamma_1/(E - \varepsilon_1) + \gamma_2/(E - \varepsilon_2) + \gamma_3/(E - \varepsilon_3)$ with $\gamma_i = \alpha_i \beta_i$ for the three MOs resulting from the simple model in Fig. 8 must also be 0. By making use of the specific symmetry properties of the 3×3 Hamiltonian in the model, we can impose $\gamma_1 + \gamma_2 + \gamma_3 = 0$ and obtain

$$E_0 = \varepsilon_1 + \frac{1}{1 + \frac{\gamma_3(\varepsilon_3 - \varepsilon_2)}{\gamma_1(\varepsilon_1 - \varepsilon_2)}}(\varepsilon_3 - \varepsilon_1) = \varepsilon_1 + F_1 F_2 \tag{2}$$

for the energy of the DQI-induced minimum, i.e., the energy E_0 defined by the condition $T(E_0) = 0$ in our model.

In Eq. (2) the factor $F_2 = \varepsilon_3 - \varepsilon_1$ is always positive by definition since the indices order the MOs in the sequence of their respective eigenenergies. Therefore, it is the sign of the other factor in the product, namely, $F_1 = 1/(1 + (\gamma_3/\gamma_1) \cdot ((\varepsilon_3 - \varepsilon_2)/(\varepsilon_1 - \varepsilon_2)))$, which decides whether the minimum

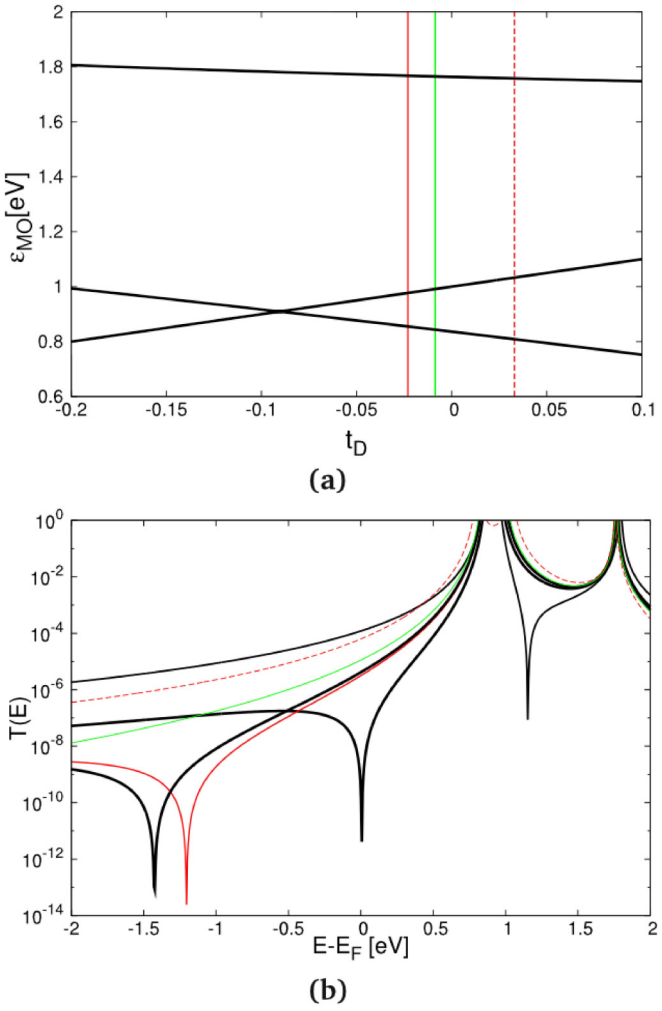

FIG. 8. (a) MO eigenenergies obtained by diagonalizing the 3×3 Hamiltonian formed by the three FOs in Fig. 7(b) with $\epsilon_L = \epsilon_R = 1.0$ eV, $\epsilon_B = 1.6$ eV, $t_L = 0.25$ eV, $t_R = -0.25$, and t_D as a variable, where the three vertical lines mark the respective t_D values of compounds m-s-l (solid red line), p-s-l (solid green line), and m-s-s (dashed red line). (b) Transmission functions calculated from $\Gamma^2(E)$ for the resulting three MOs for the t_D values of the three molecules explicitly listed in Table II and highlighted in the colors corresponding to (a) and shown as black lines for $t_D = -0.14$, -0.04, and -0.02 eV, respectively.

E_0 lies to the left or to the right of the LUMO's energy ε_1 on the energy axis. All three compounds discussed in this section have t_D values to the right of the crossing point between the lower two MO energies in Fig. 8(a), i.e., higher than $t_D = -0.09$ eV, which we obtain from Table II and list again in Table III. Within this range of t_D, γ_3/γ_1 is always positive and $F_{\text{splitting}} = (\varepsilon_3 - \varepsilon_2)/(\varepsilon_1 - \varepsilon_2)$ always negative, and therefore the product of the latter two factors must always be negative. Hence, the sign of F_1 is determined by whether this product is larger or smaller than 1; we can see from Table III that γ_3/γ_1 is fairly system independent, while $F_{\text{splitting}}$ varies widely.

For molecules m-s-l and p-s-l, where E_0, as a consequence of the negative F_1, lies to the left of the LUMO peak, the size of $F_{\text{splitting}}$ also determines how close in energy E_0 and this peak are, since F_1 scales inversely with $F_{\text{splitting}}$. The dependence

TABLE III. Explicit values for all parameters entering Eq. (2) for the three MOs obtained by diagonalizing the 3×3 Hamiltonian formed by the three FOs in Fig. 7(b) with $\epsilon_L = \epsilon_R = 1.0$ eV, $\epsilon_B = 1.6$ eV, $t_L = 0.25$ eV, $t_R = -0.25$ eV, and t_D as a variable. All values for t_D and E_0 are eV, while the factors are dimensionless.

	m-s-l	p-s-l	m-s-s
t_D	− 0.023	− 0.0087	0.033
E_0	− 1.12	− 5.58	3.49
γ_3/γ_1	0.225	0.218	0.20
$F_{\text{splitting}}$	− 6.49	− 5.24	− 3.24
F_1	− 2.16	− 6.97	2.83
F_2	0.91	0.92	0.95

of $F_{\text{splitting}}$ on t_D can be directly read from Fig. 8(a), where it can be seen that $F_{\text{splitting}}$ increases when the crossing point at -0.09 eV is approached from either side of the t_D axis. We further illustrate this point in Fig. 8(b), where we plot $\Gamma^2(E)$ in dependence on t_D and find that $T(E)$ is reproduced for the particular values for the three single-branched molecules. In addition, we also pick two characteristic values to the right of the crossing point, where it can be seen that the one approaching it more closely, at -0.04 eV, results in a DQI closer to the LUMO peak than the one farther away, at -0.02 eV, or the value for compound m-s-l (-0.023 eV). With the t_D value left from the crossing point at -0.14 eV we demonstrate that in this range γ_3/γ_1 becomes negative, which means that F_1 is always positive, thereby moving the DQI feature to energies higher than the LUMO peak, while $F_{\text{splitting}}$ then merely determines the energetic distance between the minimum and the peak.

E. Introducing the through-space coupling as an *ad hoc* parameter into conventional topological TB models

Now armed with the knowledge that the direct coupling t_D for the FO model in Fig. 7(b) reflects the structural differences most relevant for the occurrence or absence of the DQI feature below the LUMO peak for the range of molecules we investigate in this article, we return to the topological TB model we started from in Fig. 6(a) and simplify it accordingly by removing all second- and third-nearest-neighbor couplings within the anchor groups and all but one of the ferrocene FOs. In the resulting minimal topological TB model [Fig. 9(a)] we set all C and N sites at the same on-site energies for all compounds as well as using the same value for the next-nearest-neighbor couplings within all anchor groups. The single remaining ferrocene FO has an on-site energy higher than those of the AOs but also here the same value is chosen for all three systems. They now differ only in the direct coupling between the AOs in the anchor groups on opposite sides of the ferrocene closest to each other, and meta and para are also distinct in the signs of the couplings of these AOs to the bridge FO. These minimal structural differences in the model already fully reproduce the characteristic features of $T(E)$ for all molecules as can be verified from the NEGF-TB calculations presented in Fig. 9(b).

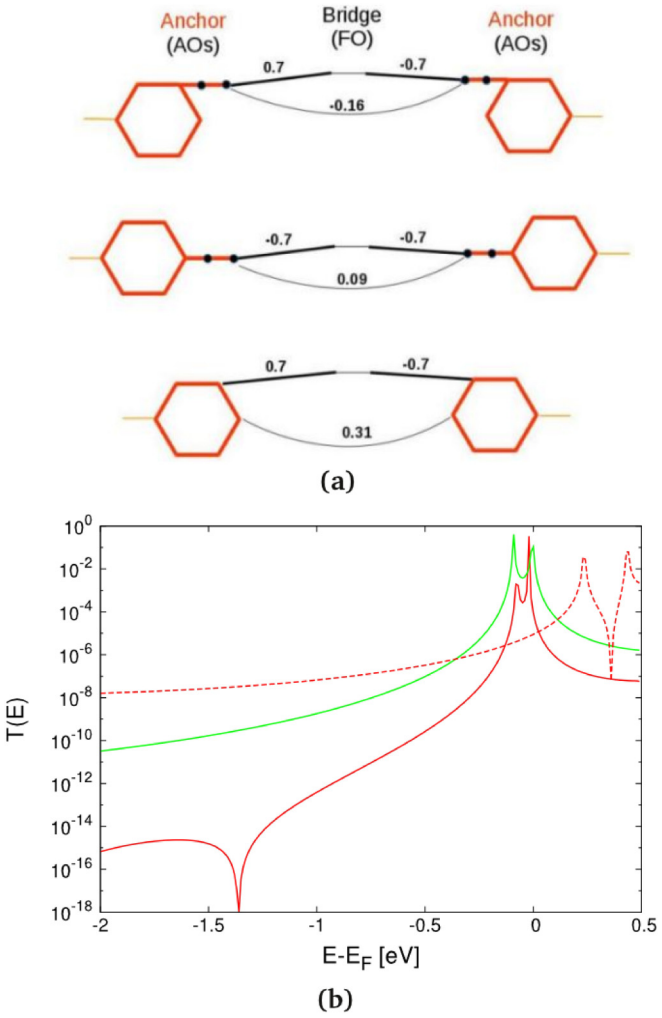

FIG. 9. (a) Conventional topological TB models for compounds m-s-l, p-s-l, and m-s-s, where only next-neighbor couplings have been considered within the pyridyl groups and acetylenic spacers, which are all set to −3.0 eV, while the coupling of the contact atom to the leads is taken to be −0.2 eV. For the on-site energies all AOs representing C and N sites are at −2.5 eV, while the single ferrocene FO is positioned at 1.7 eV for all three molecules, where only the sign of the couplings of this FO to the AOs nearest to it differs between meta and para and the value for the direct through-space coupling between anchor FOs (both given explicitly in the figure) is different for all three structures. (b) NEGF-TB calculations for the models in (a) for m-s-l (solid red line), p-s-l, (solid green line), and m-s-s (dashed red line).

F. Conclusions from the TB analysis

In summarizing this section, it can be said that molecules containing ferrocene moieties differ distinctly from planar conjugated hydrocarbons in the correspondence between molecular structure and DQI effects in electron transmission, where general rules derived from simplified topological assumptions for the latter [17,43] are not applicable to the former. Strikingly, the most important structural difference between the molecules in this study is not defined by either the meta- or the paraconnection of their respective components, the availability of almost-degenerate orbitals on the ferrocene, or the number of branches connecting the two anchor groups, although all of these aspects play a certain role in the exact energetic positioning of the DQI minimum. It is rather the direct through-space coupling between the anchor groups defined by the three-dimensional conformation of the respective compound and widely adjustable by spacer groups that determines the observability of DQI in $T(E)$ in a delicate way.

IV. EFFECT OF CHARGING OF THE BRANCHED COMPOUNDS

A. Methodology for the charging of the molecule in the junction

In this section we address the effect of the selective charging of the ferrocene center on one of the two branches in the two double-branched molecules, m-d-l and m-d-s, on the conductance in order to assess their usefulness as molecular switches along the lines suggested in Sec. I. While in experiments one of the two ferrocene moieties has to be marked by a substituent in order to achieve the asymmetry allowing for redox splitting [24], in our theoretical calculations we can achieve the same effect by making use of an idea introduced in Ref. [61], where the electronic structure of a benzene molecule was distorted in an asymmetric fashion by the strategic placement of a potassium point charge. In our work we use a method for the charging of the branched compounds with a chlorine atom in the cell close to the molecule which, due to its higher electronegativity, absorbs an electron from the junction while oxidizing it in the process [41]; the overall neutrality of the device region is still maintained. As we describe in detail in Ref. [41], where we introduced this approach for the oxidation of another organometallic complex, the generalized Δ self-consistent field technique [62,63] has to be applied in such a setup to ensure that the self-interaction problem of DFT is defied and the chloride ion is charged with one full electron while the resulting positive countercharge is distributed across the molecule and surfaces of the leads.

Following the concepts in Ref. [61] we built unit cells for the device region with a 4×8 overstructure in the surface plane in order to create some space to vary the position of the chloride ion in one direction but, with the reduction of the unit cell length along the other lattice vector, keep the computational costs at a reasonable level. Since the position of the chloride anion in the unit cell has a marked influence on the distribution of the positive charge on the molecule and surface due to electrostatic attraction [41], we vary the distance of the ion to one of the two ferrocene centers as $d_{\text{Cl-Fe}}$ (Fig. 10) in order to create asymmetry; in the following we denote the closer one Fc 1 and the one farther away Fc 2. Because of the different sizes of molecules m-d-l and m-d-s, the detailed values of $d_{\text{Cl-Fe}}$ also differ in the two cases, with values of 5.7 and 7.2 Å for the symmetric setup where the ion has an equal distance to both Fe atoms and of 4.3 and 5.4 Å where it is markedly closer to Fc 1.

B. Partial charge distributions

In Table IV we list the resulting partial charges in Fc 1 and Fc 2 as obtained from a Bader analysis [64]; it can be seen that already in the neutral cases without the presence of

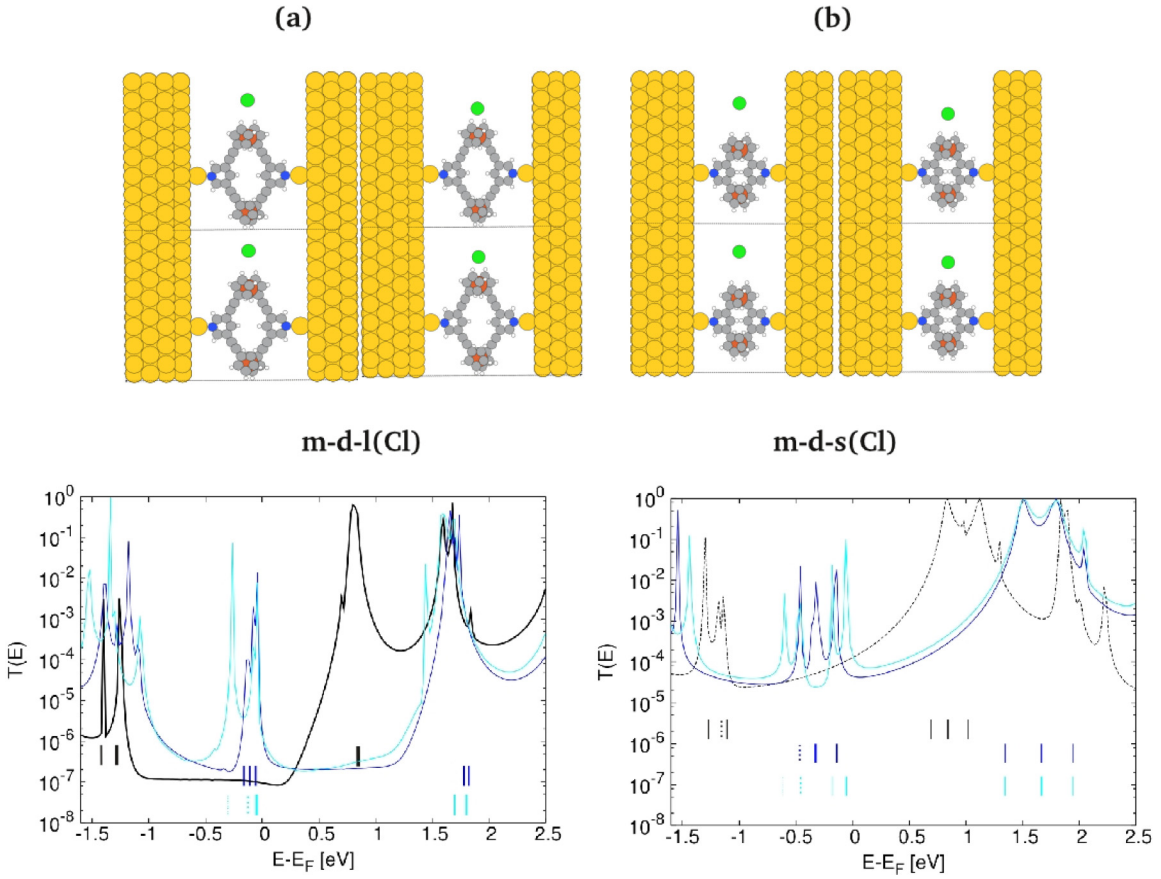

FIG. 10. Junction geometries for two neighboring cells in the periodic setup for the scattering region (upper panels) and $T(E)$ from NEGF-DFT calculations (lower panels) for the branched molecules (a) m-d-l and (b) m-d-s, where the distance $d_{\text{Cl-Fe}}$ between the Fe atom on one branch and the chloride counterion stabilizing the positive charge on the respective junction has been varied. For the transmission functions in the lower panels, which we calculated from NEGF-DFT, the neutral reference systems in the absence of charging or chlorine are represented as in Fig. 3, i.e., solid black curve for m-d-l and dashed black curve for m-d-s, while the cyan and blue curves show the $T(E)$ values for charged junctions, for asymmetric (top right panels) and symmetric (top left panels) placement of the chloride ions between the two branches in neighboring cells, respectively. The eigenenergies of the relevant MOs are also indicated in the lower panels, where the color code reflects the one used for the transmission functions and the line type distinguishes between the two branches.

the chlorine the molecules have some positive partial charges since they lose fractions of electrons to the anchor groups and the gold surfaces. When the chloride ion is introduced into the cell and a negative partial charge corresponding to one electron is enforced on it, only fractions of the resulting positive countercharge reside in the ferrocene moieties, while the partial charge on the surface changes from negative to positive (not shown here), an effect which has been discussed in terms of the respective electronegativities for another metal-organic complex in Ref. [41]. We find also a substantial accumulation of negative partial charges on the acetylenic spacers, which explains why both charges on the ferrocene groups of molecule m-d-l are consistently more than twice as large as those found for m-d-s with and without charging via the chlorine atom.

TABLE IV. Partial charges in units of fractions of 1 e as obtained from a Bader analysis [64] for the neutral and charged junctions defined in Fig. 10, where Fc 1 and Fc 2 denote the ferrocene closer to and farther away from the chloride ion, respectively. The conductance G for all junctions as defined by $T(E_F)$ in Fig. 10 is given in units of G_0.

	Fc 1	Fc 2	G
	m-d-l		
Neutral	-0.41	-0.44	0.95×10^{-7}
$d_{\text{Cl-Fe}} = 5.7$ Å	-0.61	-0.64	1.89×10^{-6}
$d_{\text{Cl-Fe}} = 4.3$ Å	-0.71	-0.55	1.41×10^{-6}
	m-d-s		
Neutral	-0.17	-0.17	1.28×10^{-4}
$d_{\text{Cl-Fe}} = 7.2$ Å	-0.28	-0.23	4.50×10^{-5}
$d_{\text{Cl-Fe}} = 5.4$ Å	-0.36	-0.18	1.57×10^{-4}

For both compounds, however, the partial charge is distinctly higher on Fc 1 than on Fc 2 in the asymmetric setup, which is also reflected by the differences in peak shifts in the respective transmission functions in Fig. 10. While the peaks in the LUMO region are almost rigidly shifted to higher energies as a consequence of the charging for both molecules, regardless of whether the ion is placed symmetrically or asymmetrically with respect to the Fe positions, there are distinct differences in the HOMO region where the asymmetry induces peak

splitting, which could be expected from the discussion in Sec. II, where we note that the HOMOs are mostly localized in the ferrocene moieties and the LUMOs in the pyridyl anchors.

C. Transmission functions and DQI for the charged compounds

Our expectation from the $T(E)$ for the neutral molecules in Sec. II was that, due to the flat behavior of the function in the HOMO-LUMO gap induced by the narrowness of the HOMO peak and DQI close to the LUMO peak, there would be almost no change in the conductance as a consequence of charging for system m-d-l, while the Lorentzian decay of the LUMO peak for m-d-s might give rise to charge-induced conductance changes since the Fermi level would move down the tail of the peak. These assumptions assumed a rigid shift of $T(E)$ and did not foresee that the HOMO-LUMO gap is reduced in size by the charging, where the tails of the HOMO peak now play a more active role in the definition of the conductance as can be seen from the NEGF-DFT calculations for the charged systems in Fig. 10, where we also list the corresponding values for G in Table IV.

It can be seen that for m-d-s the transmission functions of the neutral and the asymmetrically charged system cross each other almost exactly at E_F, resulting in almost-equal conductance values, while the conductance is enhanced by the charging for m-d-l, where the Fermi level is now at the shoulder of the HOMO peak for both the symmetric and the asymmetric setups. The latter charging effect on the conductance for m-d-l, however, would result in an on/off ratio of only ∼15–20, which is by far too low for an operative transistor. Moreover, our initial idea that the charging might have an influence on the presence or absence of DQI effects is not supported by the changes in the transmission function, although the DQI-induced flattening of the LUMO peak seems to be somewhat reduced for m-d-l in the cyan curve in Fig. 10 for the asymmetrically charged setup, where there is also a corresponding energy splitting found for the LUMO and LUMO+1, which are almost degenerate in the neutral system.

V. SUMMARY

In this study we have investigated the potential use of branched molecules containing ferrocene centers in two branches as molecular transistors, where the switching would be achieved by a redox process allowing us to alternate between an on and an off state and the latter might have a substantially reduced conductance due to DQI. We found such a DQI effect in the electron transmission for one of the branched molecules we studied in its neutral state, but this effect was not altered significantly enough by charging to enable a transistor functionality with this particular system. Quite surprisingly, the appearance of the effect was closely linked to the presence of acetylenic spacers between the ferrocene moieties and the pyridyl anchor groups. In an analysis where we mapped the essential orbital characteristics of the metal-organic compounds under investigation onto more and more simplified tight-binding models in a systematic way, we could identify the structural sources for this unexpected finding. The key quantity turned out to be the direct through-space coupling between the anchor groups, which is determined in its size and sign by the detailed three-dimensional conformation of the respective molecule. This is fundamentally different from DQI as described for planar π-conjugated hydrocarbons, where simple topological rules were derived recently and where geometrical details of the molecular structure beyond next-neighbor connectivity do not play an essential role. The systematics of our analysis in this work can be applied to other metal-organic compounds exhibiting DQI effects with an influence on their conductance and therefore provides an enabling tool for the rational design of molecular transistors.

ACKNOWLEDGMENTS

We gratefully acknowledge helpful discussions with Tim Albrecht and Michael Inkpen. All authors were supported by the Austrian Science Fund FWF (Project No. P27272). We are indebted to the Vienna Scientific Cluster, whose computing facilities were used to perform all calculations presented in this paper (Project No. 70671).

[1] M. Ratner, Nat. Nanotechnol. **8**, 378 (2013).
[2] E. Lörtscher, Nat. Nanotechnol. **8**, 381 (2013).
[3] M. Mayor, H. B. Weber, J. Reichert, M. Elbing, C. von Hänisch, D. Beckmann, and M. Fischer, Angew. Chem. Int. Ed. **42**, 5834 (2003).
[4] C. J. Lambert, Chem. Soc. Rev. **44**, 875 (2015).
[5] C. M. Guedon, H. Valkenier, T. Markussen, K. S. Thygesen, J. C. Hummelen, and S. J. van der Molen, Nat. Nanotechnol. **7**, 305 (2012).
[6] R. Stadler, S. Ami, M. Forshaw, and C. Joachim, Nanotechnology **15**, S115 (2004).
[7] T. Markussen, R. Stadler, and K. S. Thygesen, Nano Lett. **10**, 4260 (2010).
[8] T. Markussen, R. Stadler, and K. S. Thygesen, Phys. Chem. Chem. Phys. **13**, 14311 (2011).
[9] R. Stadler, Nano Lett. **15**, 7175 (2015).
[10] K. G. L. Pedersen, A. Borges, P. Hedegård, G. C. Solomon, and M. Strange, J. Phys. Chem. C **119**, 26919 (2015).
[11] K. Yoshizawa, T. Tada, and A. Staykov, J. Am. Chem. Soc. **130**, 9406 (2008).
[12] Y. Tsuji, A. Staykov, and K. Yoshizawa, Thin Solid Films **518**, 444 (2009).
[13] Y. Tsuji, A. Staykov, and K. Yoshizawa, J. Phys. Chem. C **113**, 21477 (2009).
[14] X. Li, A. Staykov, and K. Yoshizawa, J. Phys. Chem. C **114**, 9997 (2010).
[15] Y. Tsuji, A. Staykov, and K. Yoshizawa, J. Am. Chem. Soc. **133**, 5955 (2011)
[16] K. Yoshizawa, Acc. Chem. Res. **45**, 1612 (2012).
[17] X. Zhao, V. Geskin, and R. Stadler, J. Chem. Phys. **146**, 092308 (2017).

[18] R. Stadler, M. Forshaw, and C. Joachim, Nanotechnology **14**, 138 (2003).
[19] R. Stadler and T. Markussen, J. Chem. Phys. **135**, 154109 (2011).
[20] C. M. Finch, V. M. Garcia-Suarez, and C. J. Lambert, Phys. Rev. B **79**, 033405 (2009).
[21] M. Magoga and C. Joachim, Phys. Rev. B **59**, 16011 (1999).
[22] C. Joachim, Nat. Nanotechnol. **7**, 620 (2012).
[23] H. Vazquez, R. Skouta, S. Schneebeli, M. Kamenetska, R. Breslow, L. Venkataraman, and M. S. Hybertsen, Nat. Nanotechnol. **7**, 663 (2012).
[24] M. S. Inkpen, T. Albrecht, and N. J. Long, Organometallics **32**, 6053 (2013).
[25] G. Kastlunger and R. Stadler, Phys. Rev. B **91**, 125410 (2015).
[26] A. Tárraga, P. Molina, D. Curiel, and M. D. Velasco, Organometallics **20**, 2145 (2001).
[27] K. Kanthasamy, M. Ring, D. Nettelroth, C. Tegenkamp, H. Butenschön, F. Pauly, and H. Pfnür, Small **12**, 4849 (2016).
[28] C. Engtrakul and L. R. Sita, Nano Lett. **1**, 541 (2001).
[29] C. A. Nijhuits, W. F. Reus, and G. M. Whitesides, J. Am. Chem. Soc. **132**, 18386 (2010).
[30] F. Ding, S. Chen, and H. Wang, Materials **3**, 2668 (2010).
[31] S. A. Getty, C. Engtrakul, L. Wang, R. Liu, S. H. Ke, H. U. Baranger, W. Yang, M. S. Fuhrer, and L. R. Sita, Phys. Rev. B **71**, 241401 (2005)
[32] X. Xiao, D. Brune, J. He, S. Lindsay, C. B. Gorman, and N. Tao, Chem. Phys. **326**, 138 (2006).
[33] F. Schwarz, G. Kastlunger, F. Lissel, C. Egler-Lucas, S. Semenov, K. Venkatesan, H. Berke, R. Stadler, and E. Lörtscher, Nat. Nanotechnol. **11**, 170 (2016).
[34] G. Kastlunger and R. Stadler, Monatsh. Chem. **147**, 1675 (2016).
[35] F. Schwarz, M. Koch, G. Kastlunger, K. Venkatesan, H. Berke, R. Stadler, and E. Lörtscher, Angew. Chem. Int. Ed. **55**, 11781 (2016).
[36] M. Baghernejad *et al.*, J. Am. Chem. Soc. **136**, 17922 (2014).
[37] W. Hong, D. Z. Manrique, P. Moreno-García, M. Gulcur, A. Mishchenko, C. J. Lambert, M. R. Bryce, and T. Wandlowski, J. Am. Chem. Soc. **134**, 2292 (2012).
[38] R. Stadler, K. S. Thygesen, and K. W. Jacobsen, Phys. Rev. B **72**, 241401(R) (2005).
[39] R. Stadler, J. Phys.: Conf. Ser. **61**, 1097 (2007).
[40] R. Stadler, Phys. Rev. B **80**, 125401 (2009).
[41] G. Kastlunger and R. Stadler, Phys. Rev. B **88**, 035418 (2013).
[42] Y. Meir and N. S. Wingreen, Phys. Rev. Lett. **68**, 2512 (1992).
[43] D. Z. Manrique, C. Huang, M. Baghernejad, X. Zhao, O. A. Al-Owaedi, H. Sadeghi, V. Kaliginedi, W. Hong, M. Gulcur, T. Wandlowski, M. R. Bryce, and C. J. Lambert, Nat. Commun. **6**, 6389 (2015).
[44] P. Sautet and C. Joachim, Chem. Phys. Lett. **153**, 511 (1988).
[45] C. R. Arroyo, S. Tarkuc, R. Frisenda, J. S. Seldenthuis, C. H. M. Woerde, R. Eelkema, F. C. Grozema, and H. S. J. van der Zant, Angew. Chem. Int. Ed. **52**, 3152 (2013).
[46] C. Patoux, C. Coudret, J.-P. Launay, C. Joachim, and A. Gourdon, Inorg. Chem. **36**, 5037 (1997).
[47] A. Borges, E.-D. Fung, F. Ng, L. Venkataraman, and G. C. Solomon, J. Phys. Chem. Lett. **7**, 4825 (2016).
[48] M. Brandbyge, J. L. Mozos, P. Ordejon, J. Taylor, and K. Stokbro, Phys. Rev. B **65**, 165401 (2002).
[49] Y. Xue, S. Datta, and M. A. Ratner, Chem. Phys. **281**, 151 (2002).
[50] A. R. Rocha, V. M. Garcia-Suarez, S. W. Baily, C. J. Lambert, J. Ferrer, and S. Sanvito, Nat. Mater. **4**, 335 (2005).
[51] K. S. Thygesen and K. W. Jacobsen, Chem. Phys. **319**, 111 (2005).
[52] J. J. Mortensen, L. B. Hansen, and K. W. Jacobsen, Phys. Rev. B **71**, 035109 (2005).
[53] J. Enkovaara *et al.*, J. Phys. Condens. Matter **22**, 253202 (2010).
[54] A. H. Larsen, M. Vanin, J. J. Mortensen, K. S. Thygesen, and K. W. Jacobsen, Phys. Rev. B **80**, 195112 (2009).
[55] J. P. Perdew, K. Burke, and M. Ernzerhof, Phys. Rev. Lett. **77**, 3865 (1996).
[56] P. O. Löwdin, J. Chem. Phys. **18**, 365 (1950).
[57] S. Larsson, J. Am. Chem. Soc. **103**, 4034 (1981).
[58] M. A. Ratner, J. Phys. Chem. **94**, 4877 (1990).
[59] G. Kastlunger and R. Stadler, Phys. Rev. B **89**, 115412 (2014).
[60] P. Sautet and M.-L. Bocquet, Phys. Rev. B **53**, 4910 (1996).
[61] R. E. Sparks, V. M. García-Suárez, D. Zs. Manrique, and C. J. Lambert, Phys. Rev. B **83**, 075437 (2011).
[62] J. Gavnholt, T. Olsen, M. Engelund, and J. Schiøtz, Phys. Rev. B **78**, 075441 (2008).
[63] T. Olsen, J. Gavnholt, and J. Schiøtz, Phys. Rev. B **79**, 035403 (2009).
[64] W. Tang, E. Sanville, and G. Henkelman, J. Phys. Condens. Matter **21**, 084204 (2009).